Correlating AMPA Receptor Activation and Cleft Closure across Subunits: Crystal Structures of the GluR4 Ligand-Binding Domain in Complex with Full and Partial Agonists†

Avinash Gill,‡,§ Amanda Birdsey-Benson,‡,§ Brian L. Jones,|| Leslie P. Henderson,‡,|| and Dean R. Madden*,‡

Departments of Biochemistry and Physiology, Dartmouth Medical School, 7200 Vail Building, Hanover, New Hampshire 03755

Received July 12, 2008; Revised Manuscript Received November 13, 2008

ABSTRACT: AMPA receptors are glutamate-gated ion channels that are essential mediators of synaptic signals in the central nervous system. They form tetramers that are assembled as combinations of subunits GluR1−4, each of which contains a ligand-binding domain (LBD). Crystal structures of the GluR2 LBD have revealed an agonist-binding cleft, which is located between two lobes and which acts like a Venus flytrap. In general, agonist efficacy is correlated with the extent of cleft closure. However, recent observations show that cleft closure is not the sole determinant of the relative efficacy for glutamate receptors. In addition, these studies have focused on the GluR2 subunit, which is the specific target of a physiologically important RNA-editing modification in vivo. We therefore sought to test the generality of the cleft closure−efficacy correlation for other AMPA-R subunits. Here, we present crystal structures of the $GluR4_{flip}$ LBD in complex with both full and partial agonists. As for GluR2, both agonists stabilize a closed-cleft conformation, and the partial agonist induces a smaller cleft closure than the full agonist. However, a detailed analysis of LBD−kainate interactions reveals the importance of subtle backbone conformational changes in the ligand-binding pocket in determining the magnitude of agonist-associated conformational changes. Furthermore, the GluR4 subunit exhibits a different correlation between receptor activation and LBD cleft closure than does GluR2.

Within the central nervous system, most fast excitatory synaptic signals are mediated by ionotropic glutamate receptors (iGluRs) that are selective for the synthetic agonist AMPA[1] (α-amino-3-hydroxy-5-methyl-4-isoxazolepropionic acid) (*1*). In addition to their role in neurotransmission, the AMPA receptors (AMPA-Rs) contribute to synaptic plasticity and are thus thought to play important roles in learning and memory (*2*). AMPA-Rs have also been implicated in neuropathological conditions such as epilepsy, ischemia, neurodegeneration, glioma, and multiple sclerosis (*3*−*5*).

AMPA-Rs are assembled as tetramers of subunits known as GluR1−4. The composition of the receptors in a given neuron depends on which subunits are expressed, and on a variety of post-transcriptional modifications, including alternative splicing and RNA editing (reviewed in ref *1*). A particularly important modification involves the selective RNA editing of the mRNA encoding the GluR2 subunit, which converts a genetically encoded Gln codon common to all subunits to an Arg codon at position 586 in the mature sequence of GluR2. This editing is nearly 100% efficient in adults. Heteromeric channels that include edited GluR2-R subunits are the most common form of AMPA-R in vivo. They are nonrectifying and conduct predominantly monovalent cations. In contrast, AMPA-Rs that do not include GluR2-R subunits display inward rectification and are permeable to both monovalent ions and Ca^{2+}. Although less widespread, there is a growing body of evidence which shows that such Ca^{2+}-permeable AMPA-Rs play important roles in both physiological and pathophysiological processes (reviewed in refs *6* and *7*).

The GluR2 ligand-binding domain (LBD) forms a bilobate structure that binds ligands in a deep cleft located between the two lobes. High-resolution X-ray structures of multiple LBD−ligand complexes have shown that full agonists stabilize a fully closed cleft, antagonists stabilize an open cleft, and partial agonists induce intermediate degrees of cleft closure (*8*). Thus, although the ligand-free form of the core LBD exhibits some conformational flexibility (*9*), the ligand-bound GluR2 structures generally exhibit a direct correlation between the degree of cleft closure and the extent of channel activation (*10*). Recent LRET reporter assays suggest that the conformational changes seen in the isolated LBD are

† A.G. was supported in part by the John H. Copenhaver, Jr., and William H. Thomas, M.D., 1952 Fellowship Fund and by the Rosaline Borison Memorial Fund. A.B.-B. was supported by an NIH Training Grant (T32 DK07301). Financial support was provided in part by grants from the Hitchcock Foundation (to D.R.M.) and the NIH (R01-DA014137, to L.P.H.).

* To whom correspondence should be addressed: Department of Biochemistry, Dartmouth Medical School, 7200 Vail Building, Hanover, NH 03755. Telephone: (603) 650-1164. Fax: (603) 650-1128. E-mail: drm0001@dartmouth.edu.

‡ Department of Biochemistry.

§ These authors contributed equally to this work.

|| Department of Physiology.

[1] Abbreviations: iGluR, ionotropic glutamate receptor; AMPA, α-amino-3-hydroxy-5-methyl-4-isoxazolepropionic acid; AMPA-R, AMPA receptor; LBD, ligand-binding domain; NMDA, *N*-methyl-D-aspartic acid; KA, kainic acid (2-carboxy-3-carboxymethyl-4-isopropenylpyrrolidine); PEG, polyethylene glycol; NCS, noncrystallographic symmetry; CTZ, cyclothiazide.

10.1021/bi8013196 CCC: $40.75
Published on Web 12/08/2008

reflective of changes that take place in functional receptors (*11*). However, the same correlation does not hold in the case of the *N*-methyl-D-aspartate (NMDA)-selective family of ionotropic glutamate receptors. Instead, it has been observed that both full and partial agonists induce a full cleft closure of the NR1 LBD (*12*). Furthermore, a GluR2 mutation (T686A) that differentially affects the efficacies of glutamate and quisqualate without altering the extent of cleft closure seen in the isolated LBD has been identified (*13*). To account for this observation, it has been proposed that the T686A mutation destabilizes the closed versus the open cleft conformation.

While the fully edited GluR2 subunit plays an important role in the regulation of the Ca^{2+} permeability of iGluRs (*14*), the edited GluR2 subunit is poorly expressed and forms only weakly conducting ion channels by itself (*15, 16*). As a result, functional studies involving GluR2 homomers have been carried out on the GluR2-Q form, taking advantage of the fact that the electrophysiological behavior of the unedited GluR2 subunit is similar to that of the non-GluR2 subunits. To date, our understanding of the role of cleft closure in AMPA-R activation is based on this work, coupled with crystal structures of the GluR2 LBD. In contrast, structures are available for multiple members of the other major families of iGluRs (selective for NMDA and kainate) (*12, 17, 18*). As a result, it is important to assess the extent to which the relationship between cleft closure and relative efficacy is a general characteristic of AMPA-R LBDs. To address this question, we have pursued the crystallization and structure determination of the $GluR4_{flip}$ subunit.

GluR4 plays a crucial role during the early postnatal phase in the proper development of synaptic circuitry by forming functional channels in response to weak synaptic activity (*19*). GluR4 subunits are coexpressed with GluR2 in the rat subthalamic cells (*20*) and in granule cells of the cerebellum and cochlear nucleus (*21*), and GluR2 and GluR4 are known to form functional heteromeric channels (*6, 22*). Furthermore, during the development of cerebellar granule cells, expression of the $GluR4_{flip}$ isoform predominates during early development but remains relatively constant, whereas the level of expression of the $GluR4_{flop}$ isoform, which has different biophysical characteristics, increases with age (*23, 24*). Studies carried out in cultured hippocampal neurons subjected to sublethal ischemic conditions have shown a shift in AMPA-R expression patterns, characterized by increased GluR4 expression levels, and a greater permeability to Ca^{2+} ions which could lead to postischemic neuronal damage (*25*). Ultimately, GluR4 may therefore be an important therapeutic target.

Here, we present a structural analysis of the $GluR4_{flip}$ LBD core in complexes with the physiological full agonist glutamate and the partial agonist kainate (KA), together with an electrophysiological analysis of the GluR4 channel responses to these agonists. Our studies reveal a dependence of relative agonist efficacy on cleft closure that is qualitatively similar to but quantitatively distinct from that seen for GluR2. In addition, these structures allow us to analyze the compatibility of trans-subunit dimerization interactions and to investigate stereochemical differences in LBD−ligand interactions. These results emphasize the three-dimensional nature of the activation process in ligand-gated ion channels and the resulting need for high-resolution structural information for fully assembled receptors.

EXPERIMENTAL PROCEDURES

Expression Constructs. Full-length constructs for electrophysiological studies were derived from the pRK plasmid encoding the full-length $GluR4_{flip}$ glutamate receptor subunit from *Rattus norvegicus* (provided by P. Seeburg, MPI, Heidelberg, Germany). The coding sequence, which contained Ile residues at positions 713 and 834, was modified to match the published $GluR4_{flip}$ sequence [NP_058959 (*26*)], which contains Thr residues at these positions, using the QuikChange (Stratagene, La Jolla, CA) mutagenesis kit. The L484Y mutation was then introduced using the QuikChange kit. Preliminary analysis showed no significant effect of the substitutions (I713T and I834T) on the relative efficacy of kainate. The LBD construct used in crystallization studies has been described elsewhere (*27*). It contains the $GluR4_{flip}$ S1 and S2 sequences (residues 393−507 and 633−775 of the mature sequence, respectively) joined by a GT linker and subcloned into the pET16b vector (Novagen) with a thrombin cleavable polyhistidine tag. The accuracy of all constructs was verified by DNA sequencing.

LBD Purification, Crystallization, and Data Collection. Detailed expression, purification, and crystallization conditions for the GluR4 LBD construct have been reported previously (*27*). Briefly, proteins were expressed in XJB-(DE3) cells (Novagen), purified by immobilized metal affinity chromatography, and treated with thrombin to release the polyhistidine tag. The cleaved protein was collected from the flow-through of a Ni-NTA column, dialyzed extensively in crystallization buffer [10 mM HEPES-NaOH (pH 7.0), 30 mM NaCl, and 1 mM EDTA], mixed with ligand, and crystallized by vapor diffusion against 25% (w/v) PEG 4000, 0.1 M sodium acetate (pH 4.6), and 0.2 M ammonium acetate (glutamate complex) or 25.5% (w/v) PEG 1500 and 50 mM sodium acetate (pH 4.5) (kainate complex). A complete X-ray data set was collected for a GluR4 LBD−Glu crystal (at 100 K) and for a GluR4 LBD−KA crystal (at room temperature) on a MAR345dtb image plate system, using Cu Kα radiation produced by a rotating anode (Rigaku) equipped with focusing mirrors (Genova) and a Cryostream 700 (Oxford Cryosystems).

Structure Refinement. All data sets were indexed, integrated, and scaled using programs of the XDS package (*28*). Since the GluR4 LBD−Glu crystal exhibited noncrystallographic symmetry (NCS), the R_{free} test set was selected in thin shells using SFTOOLS. In the case of the GluR4 LBD−KA model, the R_{free} test set was picked by random selection using SFTOOLS. In each case, the same R_{free} set was used throughout refinement.

We first determined the structure of the GluR4 LBD−Glu cocrystal, for which the highest-resolution data were available. Initial phases were obtained by molecular replacement using CNS (*29*), with the GluR2 LBD−Glu structure [Protein Data Bank (PDB) entry 1FTJ (*30*)] as a search model. Cross rotation and translation functions yielded a final correlation coefficient of 0.67 (12−3 Å resolution) and a calculated solvent content of 54%. To minimize model bias, following rigid-body refinement, simulated annealing and composite omit map calculations were performed, together with intera-

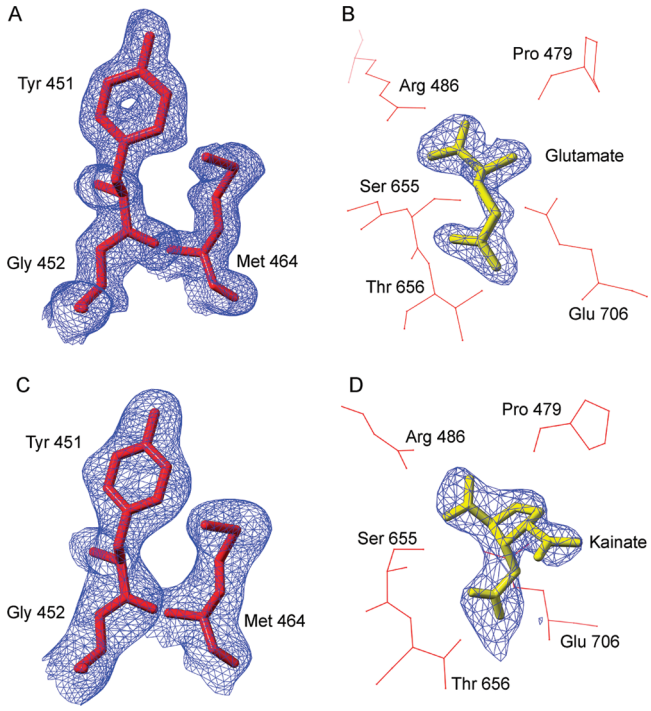

FIGURE 1: Experimental electron density for the GluR4 LBD complexes. The final refined GluR4−Glu (A) and GluR4−KA (C) structures (red stick figures) are shown together with the respective density-modified, composite omit maps (blue) used for initial model building. The glutamate (B) and kainate (D) ligands (yellow stick figures) were added to the models only after clear electron density (blue) was observed at the corresponding ligand location, following several rounds of refinement in the absence of any ligand molecule. Several of the residues surrounding the ligand molecule are shown (red stick figures). This figure was prepared using CHIMERA (*36*).

tive cycles of solvent flattening, histogram matching, and 2-fold NCS averaging, using DM (*31*).

An initial model was manually built into this iteratively averaged omit map using COOT (*32*). Refinement was carried out using a combination of the CNS and CCP4 (*33*) programs. Following manual model building, rigid-body refinement, conjugate-gradient minimization, and individual and grouped *B*-factor refinement were performed in CNS, applying strict 2-fold NCS constraints. After several rounds of refinement, a second protein molecule was generated and 2-fold NCS restraints were applied. At the stage of refinement where clear and unambiguous density was seen for the ligand in $F_O - F_C$ maps, it was added to the model (Figure 1B). Once the model was well-refined, water molecules were picked from $2F_O - F_C$ maps using PEAKMAX and WATPEAK ($>4\sigma$, <4 Å from nearest atom) and were refined after placement in the electron density map. Waters were discarded if they were unstable during refinement, if they exhibited weak density, or if they were <3.5 Å from a hydrogen-bonding partner. The final stages of refinement were carried out using TLS refinement in REFMAC5 (*34*).

To determine the structure of the GluR4 LBD−KA complex, the refined GluR4 LBD−Glu structure was used as a search model for molecular replacement calculations. Cross rotation and translation functions yielded a final correlation coefficient of 0.71 (12−3 Å resolution) and a calculated solvent content of 50%. Initial density-modified composite omit calculations, model building, and refinement of the GluR4 LBD−KA structure were carried out using the same strategy as for the GluR4 LBD−Glu model, with the exception that NCS was not present.

Domain Superpositions. LSQKAB (*35*) was used to perform superposition of the GluR4 and GluR2 LBDs. The GluR2 LBD structures used for the comparison were the GluR2 LBD−KA (PDB entry 1FWO) and GluR2 LBD−Glu (1FTJ) complexes. Residues that composed the core secondary structure elements comprising the proteins were used to define the regions of superposition. In lobe 1, GluR4 residues were matched to GluR2 residues as follows: 396−400 to 395−399, 411−415 to 410−414, 418−421 to 417−420, 424−438 to 423−437, 441−445 to 440−444, 463−469 to 462−468, 484−488 to 483−487, 489−492 to 488−491, 496−499 to 495−498, 731−739 to 730−738, and 743−756 to 742−755. For lobe 2, superpositions were based on the matching of GluR4 residues to GluR2 residues in the following order: 501−507 to 500−506, 636−642 to 635−641, 647−649 to 646−648, 655−662 to 654−661, 666−677 to 665−676, 686−696 to 685−695, 701−706 to 700−705, 707−715 to 706−714, 721−724 to 720−723, and 758−770 to 757−769. All reported cleft closure angles were calculated using LSQKAB (*35*). Linker distances were measured in CHIMERA (*36*).

tsA201 Cell Culture and Transfection. Human embryonic kidney 293 derivative cell line tsA201 (kindly provided by D. Bowie, McGill University, Montreal, QC) was grown on tissue culture dishes (Falcon) and maintained in Dulbecco's modified Eagle's medium (Mediatech) supplemented with 10% fetal bovine serum (Invitrogen), 2 mM L-glutamine, 50 IU/mL penicillin, and 50 μg/mL streptomycin (Mediatech) at 37 °C and 5% CO_2. tsA201 cells were transiently transfected with 2 μg of AMPA receptor cDNA construct and 0.8 μg of pGreenLantern plasmid (Invitrogen) using Lipofectamine 2000. Whole-cell measurements were conducted approximately 24 h after transfection. Outside-out patches were recorded after 48 h. The pGreenLantern plasmid was used as a positive transfection indicator.

Electrophysiology. L-Glutamic acid sodium hydrate (Sigma) and kainate from *Digenea simplex* (Sigma) stock solutions were prepared from solids and used within 48 h of dilution. Cyclothiazide (CTZ, Tocris) was dissolved in DMSO to form a 50 mM stock solution. CTZ was used at a final concentration of 100 μM for recordings.

Borosilicate glass pipettes with filament (Sutter Instrument Co.) were pulled and fire-polished to a final resistance, when filled, of 5−8 MΩ. All recordings were performed at room temperature (~22 °C). Whole cells and outside-out patches were voltage-clamped at −60 mV. Agonist solutions were applied as described previously (*37*) using the LSS-3100 High Speed Positioning System (Burleigh Instruments Inc., Fishers, NY), Teflon tubing, and a double-barreled theto outlet pipe with a tip diameter of 100−120 μm (Sutter Instrument Co.). Open-tip, whole-cell, and patch currents showed that 10−90% maximal on and off responses were attained in less than 2 ms. During recordings, the culture dish was perfused with a solution composed of 145 mM NaCl, 1.8 mM $MgCl_2$, 1 mM $CaCl_2$, 3 mM KCl, 10 mM glucose, and 10 mM HEPES (pH to 7.4 using NaOH). The internal pipet solution consisted of 140 mM CsCl, 2 mM $MgCl_2$, 1 mM $CaCl_2$, 10 mM EGTA, 2 mM Na_2ATP, and 10 mM HEPES (pH to 7.35 using KOH). Data were acquired using an EPC-9 amplifier and were low-pass filtered at 10

Table 1: Data Collection and Refinement Statistics

	GluR4 LBD−L-glutamate	GluR4 LBD−kainate
conditions	100 K, flash-cooled	room temperature, capillary-mounted
space group	$P2_1$	$C2$
unit cell parameters	a = 47.4 Å, b = 105.1 Å, c = 66.6 Å, β = 97.3°	a = 125.9 Å, b = 48.8 Å, c = 47.8 Å, β = 109.1°
Matthews coefficient (Å^3/Da)	2.67	2.32
solvent content (%)	53.6	49.4
resolution[a]	19.51−1.85 (1.93−1.85)	11.95−2.43 (2.49−2.43)
total no. of reflections[a]	202326 (23356)	38423 (2663)
no. of unique reflections[a]	52938 (6140)	10025 (681)
R_{sym} (%)[a,b]	8.9 (17.5)	10.9 (35.7)
completeness (%)[a]	96.3 (94.1)	95.3 (94.1)
Refinement Statistics		
no. of protein atoms (non-H)	4028	2014
no. of waters	310	97
R_{work} (%)[a]	19.1 (18.6)	16.2 (21.6)
R_{free} (%)[a]	22.0 (24.0)	21.9 (29.0)
I/σ_I[a]	11.5 (7.1)	9.2 (4.1)
Ramachandran plot[c] (%)	93.3/6.7/0/0	94.2/5.8/0/0
rmsd (bonds/angles)	0.009 Å/1.125°	0.008 Å/1.167°
protein B_{av} (Å^2)[d] (chain A/B)	12.45 (12.48/12.42)	43.58 (N/A)
ligand B_{av} (Å^2)[d] (chain A/B)	5.7 (5.9/5.6)	30.91 (N/A)
water B_{av} (Å^2)[d]	14.42	46.37

[a] Values in parentheses indicate statistics for the highest-resolution shell of data. [b] $R_{sym} = \sum_{hj}|\hat{I}_h - I_{hj}|/\sum_{hj}I_{hj}$. [c] Core/allowed/generously allowed/disallowed. [d] Residual B factors calculated with REFMAC (does not include the contribution to atomic displacements from translation, libration, and screw-rotation displacement).

kHz. Between two and five current responses with a duration of 100 ms each were averaged for subsequent analysis of peak current (I_{peak}) using HEKA Pulse and PulseFit (Instrutech Corp.).

RESULTS AND DISCUSSION

In this study, crystal structures have been determined for the GluR4 LBD in complex with the physiological agonist glutamate and in complex with the partial agonist kainate (Table 1). The presence of noncrystallographic symmetry in the GluR4 LBD−Glu crystals provided a strong basis for reducing model bias following phase determination by molecular replacement. The electron density in iteratively averaged composite omit maps was of excellent quality and permitted direct modeling of the GluR4 LBD core structure (Figure 1A). After several rounds of refinement at 1.85 Å resolution, the density for the bound glutamate ligand was also of excellent quality (Figure 1B), and ligand was incorporated into the model. The final model consists of 514 residues in two molecules, with a bound glutamate ligand for each, and a total of 310 water molecules (Table 1). The root-mean-square (rms) difference between the two chains in the asymmetric unit is 0.18 Å, consistent with a highly conserved, stable structure. The refined GluR4 LBD−Glu model was used without ligand as a molecular replacement search model for the GluR4 LBD−KA complex. Density-modified composite omit maps were again unambiguous (Figure 1C). The structure was refined at 2.43 Å resolution. As was the case for the glutamate complex, clear density for the bound kainate ligand emerged during refinement (Figure 1D) and was fit accordingly. The final kainate model consists of 257 residues, a bound kainate ligand, and 97 water molecules (Table 1). The resulting models provide insights into the structure of an additional AMPA receptor subunit and permit comparison with the previously determined GluR2 LBD structures. Coordinates of the GluR4 LBD−Glu and GluR4 LBD−KA models have been deposited in the Protein Data Bank, as entries 3EPE and 3EN3, respectively.

In complex with either glutamate (Figure 2A,C, red) or kainate (Figure 2B,C, blue), the GluR4 LBD exhibits a bilobate structure with a deep ligand binding cleft between the two lobes, similar to that observed in other members of the iGluR family, and in the homologous bacterial glutamine binding protein (reviewed in ref *10*). Superposition of the glutamate-bound forms of the GluR4 and GluR2 LBD showed that they are very similar (Figure 2A, red and gray, respectively), in terms of both the individual lobes and the overall structure, with rms differences ranging from 0.2 to 0.3 Å. The kainate-bound structures of the GluR4 and GluR2 LBD (Figure 2B, blue and gray, respectively) show slightly higher rms differences (0.3−0.5 Å) but remain very similar overall.

Trans-Subunit Compatibility of Dimerization Interfaces. The protein chains in GluR4 LBD agonist cocrystals pack in a back-to-back fashion to form a 2-fold symmetric dimer (Figure 3A). The dimerization interface consists of hydrogen bonds, hydrophobic interactions, and van der Waals interactions and is mediated between opposing faces of the membrane-distal, i.e., N-terminal, lobes of each LBD (lobe 1). A similar arrangement has been seen in several of the GluR2 LBD−ligand cocrystals (Figure 3B) and has been shown to play an important role in the gating and desensitization of the receptors (*38*).

The LBD dimer is thought to be incorporated within the framework of a dimer-of-dimers assembly of intact iGluR subunits (reviewed in ref *10*). However, in the absence of structural information for other subunits that comprise physiological, heteromeric AMPA-Rs, it has not been possible to assess directly the compatibility of the interfaces. In addition, alternative splicing of GluR1−4 subunit mRNAs produces either "flip" or "flop" versions of the subunits, which exhibit distinct activation and desensitization characteristics (*26*). Finally, in GluR2, GluR3, and GluR4, an RNA editing site is located just before the flip−flop cassette (*39*). The presence of either a Gly or an Arg at this "R/G" site also determines key biophysical properties of receptors

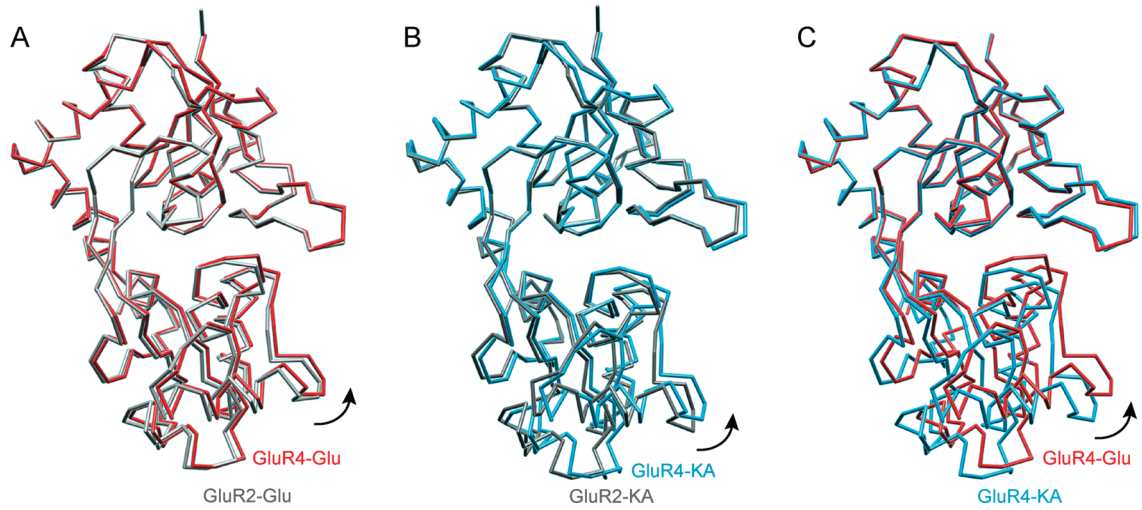

FIGURE 2: Comparison of cleft closure in GluR4 and GluR2 ligand-bound structures. (A) Superposition of glutamate-bound GluR4 LBD (red) and GluR2 LBD (gray) structures. (B) Superposition of the kainate-bound GluR4 LBD (blue) and GluR2 LBD (gray) structures. (C) Superposition of GluR4 LBD structures bound to glutamate (red) and kainate (blue). The Glu-bound structure shows a greater degree of cleft closure than the kainate-bound structure (difference of ~6.7°). In each case, the core residues of lobe 1 were superimposed. This figure was prepared using CHIMERA (*36*).

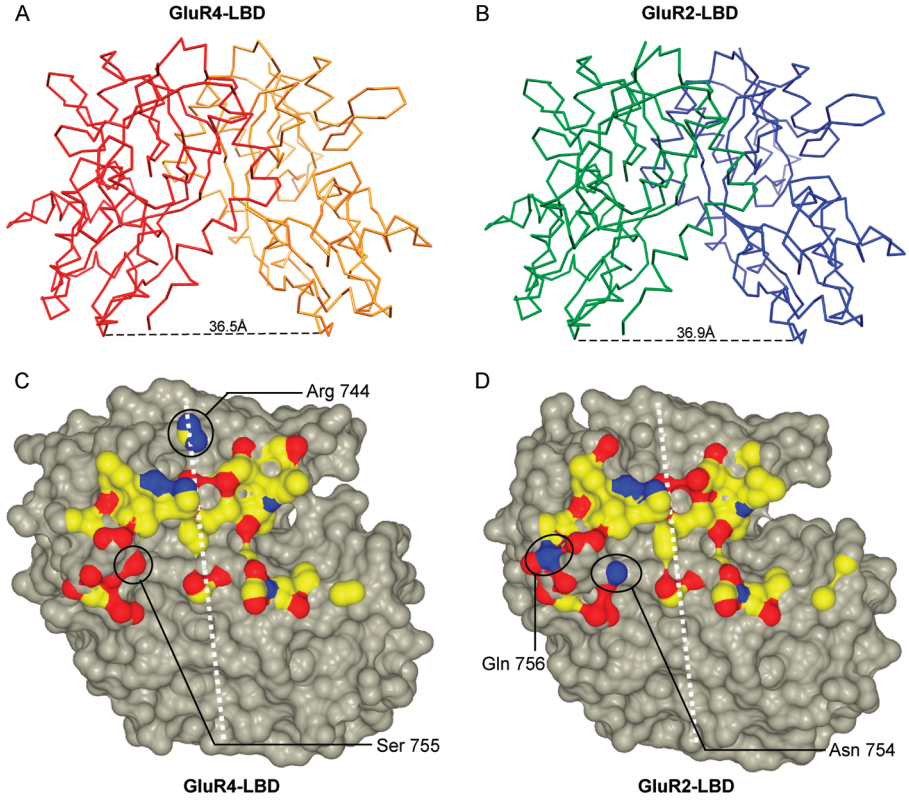

FIGURE 3: Conservation of the GluR2 and GluR4 dimerization interfaces. C_α traces of the GluR4 LBD−Glu (A) and GluR2 LBD−Glu (B) dimers are shown with the distances between Gly C_α atoms in the Gly-Thr linker depicted at the bottom. The buried surfaces involved in the homodimer interfaces of the GluR4 LBD (C) and the GluR2 LBD (D) are also shown for a single subunit. In each case, the dimer 2-fold axis is shown as a white dashed line. The surface of the residues buried in the interface is colored by atom type (yellow for carbon, red for oxygen, and blue for nitrogen). The surfaces of atoms not involved in the dimer interface are colored gray. The footprint of the dimer interface is similar for GluR2 and GluR4, as is the stereochemistry, with the exception of solvent-exposed residue Arg744 and $GluR4_{flip/R}$ residues Ser755 and Ala757, which replace $GluR2_{flop/G}$ residues Gly743, Asn754, and Gln756, respectively (circled). This figure was prepared using CCP4MG (*55*).

containing these subunits (*40*). Despite this diversity, with the exception of PDB entry 2UXA (*41*), all published crystal structures have been determined for the flop version of GluR2, with a Gly at the R/G site.

The form of GluR4 that has been crystallized in this study is the flip variant, with an Arg at the R/G site. A superposition of the glutamate-bound GluR4 and GluR2 LBD dimers reveals only a 0.4 Å rms difference (Figure 3A,B). This value is comparable to the 0.2−0.3 Å rms differences between LBD monomers, suggesting a highly similar dimerization interaction. A comparison of the buried surface of the $GluR4_{flip/R}$ dimer interface (Figure 3C) with that of the $GluR2_{flop/G}$ interface (Figure 3D) reveals a high level of stereochemical compatibility. Since these domains each can

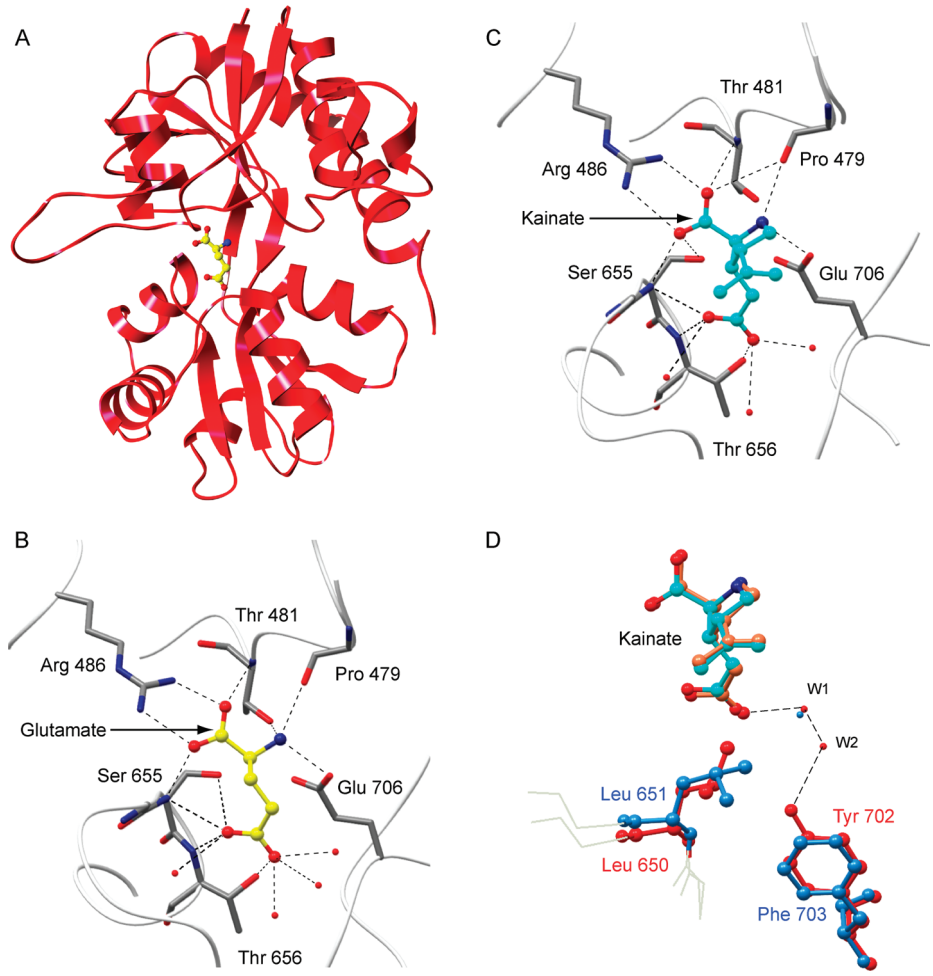

FIGURE 4: GluR4 LBD−ligand interactions. (A) Ribbon diagram for the GluR4 LBD bound to glutamate. Close-up views of the ligand-binding pockets show contacts between the glutamate (B, yellow) or kainate (C, cyan) ligands and the surrounding amino acids in each binding cleft. This view of the ligand-binding cleft is in the same orientation of the model as presented in panel A. Ligands are depicted in ball-and-stick representation, colored by atom type (white or yellow for carbon, red for oxygen, and blue for nitrogen). Water molecules are shown as red spheres. Hydrogen bonds are illustrated with dashed lines. Tyr451 is located in front of the plane of the figure in this orientation and has been omitted for the sake of clarity. (D) Close-up view of the ligand-binding pocket shown following superposition of the GluR2 and GluR4 LBD structures in complex with kainate. Protein residues (stick figures) and water molecules (spheres) belonging to the GluR4 chain are colored blue, and those belonging to the GluR2 chain are colored red. Kainate bound to GluR4 is colored cyan, while the GluR2-bound kainate is colored coral. The dashed lines depict water-mediated hydrogen bonds formed between Tyr702 and kainate in the GluR2 LBD structure. This figure was prepared using CHIMERA (*36*) and CCP4MG (*55*).

form homodimers (2-fold axis shown in white, Figure 3C,D), their similarity is also consistent with the ability of the two different subunits and splice variants to form heteromeric channels in vivo (*20, 21*). In particular, there is a pair of conserved salt bridges between Glu487 on one chain and Lys594 on the opposite chain, as well as a conserved hydrogen bond between Asn748 and Glu487 (GluR4 numbering). Leu484, a residue which blocks desensitization when mutated to a Tyr in GluR3 (*42*), maintains a set of hydrophobic contacts similar to those seen in GluR2 (*38*). Even where stereochemical differences are observed (Figure 3C,D, circled), interface compatibility is generally preserved. For example, in $GluR2_{flop}$, Asn754 makes a direct hydrogen bond with Ser729 on the opposite chain. In the case of $GluR4_{flip}$, the corresponding Ser755 makes a water-mediated hydrogen bond with Ser730 on the protein chain across the dimer interface. At the edge of the interface, Gln756 in $GluR2_{flop}$ is replaced with Ala757 in $GluR4_{flip}$.

The other major stereochemical difference involves Arg744 at the R/G editing site (Figure 3C, circled). Surprisingly, the terminal guanidino groups of the two Arg side chains point toward each other, with N_η groups only 3.1 Å apart. A similar arrangement has been observed in the $GluR2_{flip}$ structure (*41, 43*). There are no stabilizing lattice contacts in the vicinity in either the $GluR4_{flip}$ structures reported here or the $GluR2_{flip}$ structure (PDB entry 2UXA). A possible explanation involves the presence of a set of conserved negatively charged or polar residues in the vicinity (*41*), as well as the fact that the side chains are partially solvent exposed. In the case of GluR2, Arg743 promotes homotetramerization, efficient folding, and ER budding (*41*). However, it remains possible that Arg−Gly interactions may also act to favor heterotetramerization across subunits.

Stereochemistry of Ligand Binding. The GluR4 LBD binds to its full agonist glutamate (Figure 4A,B) and partial agonist kainate (Figure 4C) in a manner similar to that seen for the GluR2−ligand cocrystal structures (*30*). In particular, in both of the GluR4 LBD structures, the α-carboxyl and α-amino groups of glutamate and kainate interact with side chains of conserved residues surrounding the cleft, Arg486, Thr481, and Pro479 in lobe 1 and Ser655 and Glu706 in lobe 2, in a manner that agrees very well with that seen previously for

other iGluR family members (Figure 4B,C). This observation is consistent with the 89% level of sequence identity between the domains. It validates the assumptions underlying our previous homology-based analysis of GluR4−ligand binding energetics using FTIR spectroscopy (*44*−*46*). It also confirms the structural basis of the analysis of GluR4 LBD−agonist interaction kinetics, which revealed a two-step binding process (*47*).

Interactions of the LBD binding pocket with agonist side chain moieties are also strongly conserved. Ser655 and Thr656 both form hydrogen bonds (Figure 4B,C), while Leu651 acts as a "foot in the door" for the kainate isopropenyl group (Figure 4D). In addition, as seen in GluR2 LBD−ligand complexes (*30*), a number of water molecules are seen to interact with the agonist side chains in the binding cleft, providing stereochemical flexibility for the accommodation of different agonists and antagonists (Figure 4B,C). However, this water network is generally conserved as well. Within a hydrogen bonding distance of the bound kainate ligand, there are three water molecules in both GluR2 and GluR4 structures, all of which overlap.

Comparison of the glutamate- and kainate-bound structures reveals a different degree of cleft closure for each complex (Figure 2C). As seen with the binding of partial and full agonists to GluR2, GluR5, and GluR6 (*17, 18, 30*) but not to NR1 (*12*) LBD, the full agonist glutamate induces a more compact structure of the GluR4 LBD than does the partial agonist kainate (Figure 2C). Even though an apo or antagonist-bound crystal structure is not available for the GluR4 LBD, small-angle X-ray scattering studies have previously shown that the full-length GluR4 LBD is more compact in the presence of full agonist glutamate or AMPA than it is in the apo state or in complexes formed with competitive quinoxaline antagonists (*9*). Thus, given that kainate is a partial agonist for GluR4 (*48*), the qualitative correlation between cleft closure and relative agonist efficacy, originally identified for the GluR2 LBD, appears to be conserved at least for the non-NMDA iGluRs.

Differential Relationship between Relative Efficacy and Cleft Closure. Despite this qualitative similarity, there are differences in the relative degrees of cleft closure seen in GluR2 versus GluR4. Specifically, while the GluR2 LBD cleft is 8.9° more closed in the presence of glutamate than in the presence of kainate, for the GluR4 LBD, the difference is only 6.7°. In other words, in GluR4, the kainate-bound LBD structure is ∼2° closer to the glutamate-bound structure than is the case for GluR2. Previously, an increase of only 3° in GluR2 LBD cleft closure was proposed to account for an increase in the relative efficacy of kainate from 2 to 24% (*49*). As a result, we tested whether the greater relative cleft closure associated with kainate binding to the GluR4 LBD corresponds to a similarly enhanced relative efficacy.

Like other AMPA-Rs, wild-type (WT) GluR4 homomeric receptors exhibit fast desensitization kinetics, making it difficult to measure peak currents accurately (Figure 5A). A point mutation in the dimer interface that converts a Leu (position 483 in GluR2) to a Tyr is known to inhibit desensitization in the GluR1, GluR2, and GluR3 subunits (*38, 42*). To test whether the homologous mutation would have a similar effect in GluR4, we generated an expression vector encoding the full-length GluR4 subunit with the L484Y mutation and measured the responses to glutamate and to

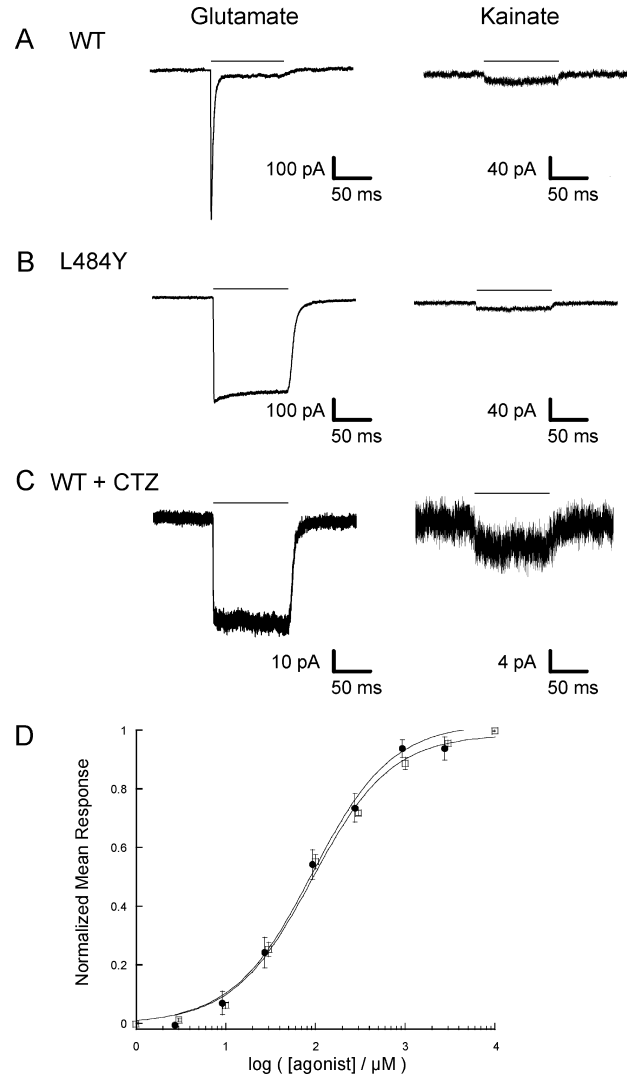

FIGURE 5: Kainate is a weak partial agonist of GluR4. (A) The response of a representative outside-out patch to a 100 ms pulse of 10 mM glutamate (left) or kainate (right) for GluR4-WT (A and C) and GluR4-L484Y (B) receptors in the absence (A and B) or presence (C) of 100 μM cyclothiazide. The horizontal bar represents the time of agonist application. Traces for kainate (right) are scaled up 2.5 times relative to traces for glutamate (left). (D) Normalized dose−response curves for GluR4-L484Y using kainate (●) and glutamate (□). Curves were acquired using whole-cell voltage-clamp recordings. Data were fit using the Hill equation $y = I_{max}[x^n/(k^n + x^n)]$, where $y = I/I_{max}$, I_{max} is the maximum current amplitude, x is the agonist concentration, n is the Hill coefficient, and k is the EC_{50}.

kainate in GluR4-L484Y homotetramers. As shown in Figure 5B, the GluR4-L484Y mutation has the expected effect, dramatically decreasing the extent of desensitization and permitting more reliable assessment of agonist-induced peak currents.

A dose−response analysis of currents elicited by 100 ms pulses of kainate or glutamate acting on the L484Y receptor showed similar EC_{50} values for kainate and glutamate [92 ± 14 and 92 ± 10 μM, respectively (Figure 5D)]. Hill coefficients were close to unity for both kainate (0.98 ± 0.12) and glutamate (0.99 ± 0.09). To determine the relative peak current ratio of kainate to glutamate, outside-out patches of tsA201 cells expressing GluR4-L484Y subunits were exposed to 100 ms pulses of buffer containing 10 mM glutamate or 10 mM kainate (i.e., ∼100 × EC_{50}). For each

patch, two to five individual responses were averaged, and the ratio of I_{peak} in response to kainate versus I_{peak} in response to glutamate was determined. This ratio was 2.7 ± 0.4% (n = 5) for cells expressing GluR4-L484Y subunits, which is very similar to the value of 2% reported for GluR2-L483Y receptors (*49*). CTZ is a pharmacological agent that provides an alternative means of suppressing AMPA-R desensitization and has also been used in studies of GluR2 agonist responses (*49*). As seen with GluR2 receptors, CTZ suppresses desensitization of GluR4 receptors more strongly than does the L484Y mutation (Figure 5C). In the presence of CTZ, the ratio of kainate- to glutamate-induced peak currents was 7.8 ± 0.1% (n = 8), well below the value of 17% observed for GluR2 receptors under comparable conditions (*49*).

Thus, despite the greater degree of relative cleft closure in GluR4, kainate remains a very weak partial agonist in comparison to glutamate, with relative efficacy less than or equal to that seen with GluR2 channels. These data stand in contrast to the observations made with the GluR2-L650T channels, which indicated that a few additional degrees of cleft closure can significantly enhance efficacy (*49*). As a result, the slope of the line relating efficacy to the rotation angle of cleft closure appears to be different for the GluR2 and GluR4 subunits. Indeed, as shown in Figure 6A, the line is shallower for GluR4 than it is for GluR2 and is thus intermediate between those of GluR2 and NR1, for which the slope is close to zero (*12*). An alternative representation for the extent of cleft closure is the separation between the two linker peptides in the LBD dimer. This corresponds roughly to the separation between the attachment points that connect to the first two transmembrane domains of a pair of subunits in the receptor. When plotted for the GluR2 and GluR4 glutamate and kainate structures (Figure 6B), the difference in slope is even more dramatic. Glutamate binding to GluR2 drives an increase in linker separation of 2.6 Å more than kainate. In contrast, glutamate binding to GluR4 drives an increase in linker separation of only 0.9 Å compared to that of kainate. Nevertheless, the relative efficacy difference between kainate and glutamate is very similar for homomeric receptors composed of either subunit.

One interpretation of our data is that different subunits exhibit a different sensitivity or "gain" when converting cleft closure or linker separation into channel activation. Such differences could reflect the three-dimensional structure of the coupling and gating mechanisms of intact subunits or receptors. Indeed, the fact that changes in linker separation do not strictly track cleft closure (Figure 6B) suggests that the relationship between lobe closure and transmembrane connector spacing is itself complex. Another interpretation is that relative destabilization of the kainate-bound GluR4 LBD reduces the net efficacy of the partial agonist in a way that compensates for enhanced activation via greater cleft closure. Finally, as discussed below, the stereochemistry of the GluR4 ligand-binding site accommodates the greater degree of kainate-associated cleft closure observed. Nevertheless, although analysis of lattice effects on GluR2 LBD cleft closure suggests that they are modest (*50*) and our crystallographically independent Glu-bound protomers are extremely similar, it remains a formal possibility that crystal contacts may also contribute to the precise conformations observed. In any case, it is clear that there is not a single parameter governing the conversion of crystallographically

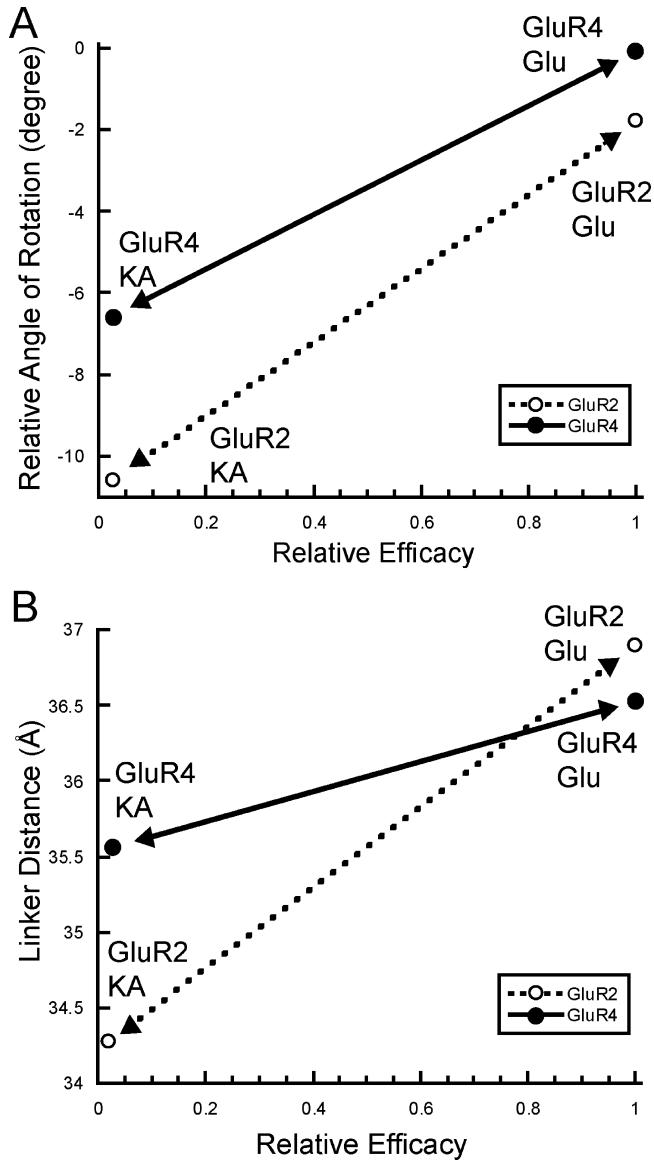

FIGURE 6: Differential relationships between relative agonist efficacy and LBD conformational changes in GluR4 and GluR2. (A) Plot of the degree of cleft closure vs agonist efficacy for kainate- and glutamate-bound forms of both LBDs. Following superposition of lobe 1 of the GluR4 LBD−KA, GluR2 LBD−KA (1FWO), or GluR2 LBD−Glu (1FTJ) complex onto lobe 1 of the GluR4 LBD−Glu complex, the relative angle of rotation required to superimpose lobe 2 of the structures onto lobe 2 of the GluR4 LBD−Glu complex was determined. Negative values indicate a more open cleft. (B) Graph plotting linker distances (as measured between glycine C_α atoms in the GT linker) vs agonist efficacy for the same set of structures. To illustrate the relative slope, lines with arrows are shown connecting the kainate- and glutamate-bound points for GluR4 (solid) and GluR2 (dashed).

observed LBD cleft closure to channel activation across AMPA-R subunits. Ultimately, these differences may be important in determining the physiological effects of AMPA-R modulatory compounds as a function of subunit composition.

Structural Basis of Differential Cleft Closure. In principle, the difference in relative cleft closure between kainate and glutamate for GluR2 versus GluR4 could reflect differences in either the kainate- or glutamate-bound states, or both. As shown in Figure 6A, it is clear that both ligand complexes are more closed for the GluR4 LBD than are the correspond-

ing complexes with the GluR2 LBD. However, the difference between the glutamate-bound GluR4 and GluR2 structures [1.8° (Figure 2A)] is smaller than that between the kainate-bound forms [4.2° (Figure 2B)]. Remarkably, even though the GluR4 LBD−Glu structure is slightly more closed than the GluR2 LBD−Glu structure, the relationship between the linker distance is inverted, with the GluR2 LBD exhibiting a greater linker separation (36.9 Å, vs 36.5 Å for GluR4). In contrast, the GluR4 LBD−KA linker separation (35.6 Å) is significantly larger than that of the GluR2 LBD−KA complex [34.3 Å (Figure 6A)] even though kainate is a similarly weak partial agonist for both subunits. In fact, the GluR4 LBD−KA linker separation is greater than the GluR2 L650−KA separation (35.3 Å), which is associated with a significantly higher relative kainate efficacy of 24% (*49*). Such differences between GluR2 and GluR4 again underscore the danger of an overly linear interpretation of three-dimensional conformational transitions. The variability in cleft closure and linker separations also suggests that additional flexibility may be observed in other subunits and in complexes with other ligands.

What accounts for the nearly 4° difference in cleft closure between the kainate-bound forms of GluR2 and GluR4? A key determinant of the extent of cleft closure is the side chain at position 651 (650 in GluR2) (*49*). The isopropenyl group of the kainate side chain would clash sterically with Leu651 if the GluR4 LBD were in the glutamate-bound conformation with kainate in the binding pocket. To prevent this clash, when kainate is bound, the cleft closes less tightly. However, GluR2 and GluR4 both have a Leu side chain at position 650/651. The essential difference in cleft closure is thus accommodated not by a change in the covalent structure of the LBD but rather by a reorientation of the terminal methyl groups of the Leu side chain. Whereas these point toward the ligand in GluR2 and thus impose a more open structure, in GluR4 they are oriented away from the ligand, allowing a greater degree of closure (Figure 4D).

This reorientation is at least in part facilitated by the replacement of Tyr702 in GluR2 with Phe703 in GluR4. In GluR2, the hydroxyl group of Tyr702 makes contact with kainate via water-mediated hydrogen bonds (Figure 4D, W1 and W2, red spheres), one of which (W2) is found only in the GluR2 structure (*30*). At the same time, the hydroxyl group prevents the more streamlined orientation of Leu650. In contrast, in the GluR4−KA structure, replacement of Tyr702 with Phe703 creates a hydrophobic surface against which the methyl groups of Leu651 can pack. While lattice contacts may influence the exact extent of cleft closure observed (*50*), this ability of the Leu side chain to reorient ultimately permits the GluR4 LBD to close more than the GluR2 LBD, an absolute prerequisite for the smaller conformational difference between these full and partial agonist-bound forms of GluR4.

Interestingly, the replacement of Tyr702 with a Phe is not by itself sufficient to allow the reorientation of the Leu650 side chain, as shown by Frandsen et al. (*51*). While the GluR2-Y702F mutation did increase the degree of cleft closure slightly, it did not cause a reorientation of the Leu650 terminal methyl groups. Instead, the increase was attributed to the creation of a more hydrophobic region surrounding residue 702, leading to a shift of bound water molecules and a tighter interaction between residues that provided the interdomain lock, as well as to the different conformation of Ser654 (*51*). Analysis of the GluR2-Y702F LBD structure in complex with KA shows that if Leu650 of GluR2 were oriented away from kainate, as Leu651 is in GluR4, a modest steric clash could still occur between Leu650 and Phe702, due to differences in the backbone orientation between the two subunits. On the other hand, if the terminal methyl groups of Leu651 were to be oriented in the same manner in GluR4 as they are in GluR2-Leu650, then a steric clash between the isoproprenyl group of kainate and Leu651 would occur, indicating that the side chain at Leu651 is not free to reorient itself away from Phe703. Our results highlight the potential limitations of focusing exclusively on the residues that directly interact with a ligand. Instead, in this case, it is a combination of side chain substitutions and backbone rearrangements that permit the differential cleft closure. Both of these differences involve "second-shell" residues, i.e., the residues that do not directly interact with the ligand but affect the stereochemistry of the binding site.

Such second-shell residues could potentially also play a role in the binding of GluR4-selective pharmacological agents. Agonists such as 6-aza-substituted willardiine derivatives display an increased potency for GluR4 receptors (*52, 53*), and others like 2-Bn-Tet-AMPA exhibit a 40-fold increased potency for GluR4 receptors compared to GluR1 and -2 receptors (*54*). An examination of the ligand-binding subpockets in the vicinity of the functional groups that are changed did not show any obvious stereochemical differences between GluR4 and GluR2 structures that would account for these results. Instead, it is likely that small sequence differences in second-shell or other residues might provide some torsional flexibility that helps with accommodation of these subtype-selective agonists. A fuller understanding of the subtype selectivity of such pharmacological compounds is therefore likely to require cocrystal structures for these agonists with both GluR4 and GluR2.

CONCLUSION

The structures of the $GluR4_{flip}$ LBD in complex with an agonist and partial agonist permit a comparison of conformational changes across subunits of the AMPA-R family of ion channels. The electrophysiological behavior of GluR4 follows the trend that has been observed for the GluR2 subunit, showing a positive correlation between cleft closure and agonist efficacy. On the other hand, comparative analysis of GluR4 structures with previously determined GluR2 structures shows that the slope of this correlation is different and has distinct consequences in terms of the potential separation of transmembrane domains within a subunit pair. It is likely that activation is dictated not simply by a set of linear extrapolations, but by a complex, three-dimensional conformational rearrangement that will require detailed structural analysis of intact iGluR. Our findings also emphasize the potential contributions of subtle ligand binding interactions that govern subunit-selective interactions with ligands or modulators. Ultimately, it will be important to focus on the structural analysis of heteromeric subunit combinations that more accurately reflect the composition of physiological AMPA-Rs. In the meantime, comparative analysis of multiple individual subunits provides an opportunity to distinguish subunit-specific from general characteristics of this important family of neurotransmitter receptors.

ACKNOWLEDGMENT

We thank Dr. P. Seeburg (MPI) for the initial GluR4 wild-type expression vector, Dr. D. Bowie (McGill University) for the tsA201 cell line, and Dr. C. Panetti, Dr. R. Maue, and Dr. J. Kull (Dartmouth Medical School) for helpful discussions.

REFERENCES

1. Dingledine, R., Borges, K., Bowie, D., and Traynelis, S. F. (1999) The glutamate receptor ion channels. *Pharm. Rev. 51*, 7–61.
2. Derkach, V. A., Oh, M. C., Guire, E. S., and Soderling, T. R. (2007) Regulatory mechanisms of AMPA receptors in synaptic plasticity. *Nat. Rev. Neurosci. 8*, 101–113.
3. Newcombe, J., Uddin, A., Dove, R., Patel, B., Turski, L., Nishizawa, Y., and Smith, T. (2008) Glutamate Receptor Expression in Multiple Sclerosis Lesions. *Brain Pathol. 18*, 52–61.
4. Lipton, S. A., and Rosenberg, P. A. (1994) Excitatory Amino Acids as a Final Common Pathway for Neurologic Disorders. *N. Engl. J. Med. 330*, 613–622.
5. Sontheimer, H. (2003) Malignant gliomas: Perverting glutamate and ion homeostasis for selective advantage. *Trends Neurosci. 26*, 543–549.
6. Cull-Candy, S., Kelly, L., and Farrant, M. (2006) Regulation of Ca^{2+}-permeable AMPA receptors: Synaptic plasticity and beyond. *Curr. Opin. Neurobiol. 16*, 288–297.
7. Liu, S. J., and Zukin, R. S. (2007) Ca^{2+}-permeable AMPA receptors in synaptic plasticity and neuronal death. *Trends Neurosci. 30*, 126–134.
8. Oswald, R. E. (2004) Ionotropic glutamate receptor recognition and activation. *Adv. Protein Chem. 68*, 313–349.
9. Madden, D. R., Armstrong, N., Svergun, D., Perez, J., and Vachette, P. (2005) Solution X-ray scattering evidence for agonist- and antagonist-induced modulation of cleft closure in a glutamate receptor ligand-binding domain. *J. Biol. Chem. 280*, 23637–23642.
10. Madden, D. R. (2002) The structure and function of glutamate receptor ion channels. *Nat. Rev. Neurosci. 3*, 91–101.
11. Gonzalez, J., Rambhadran, A., Du, M., and Jayaraman, V. (2008) LRET investigations of conformational changes in the ligand binding domain of a functional AMPA receptor. *Biochemistry 47*, 10027–10032.
12. Inanobe, A., Furukawa, H., and Gouaux, E. (2005) Mechanism of Partial Agonist Action at the NR1 Subunit of NMDA Receptors. *Neuron 47*, 71–84.
13. Zhang, W., Cho, Y., Lolis, E., and Howe, J. R. (2008) Structural and Single-Channel Results Indicate That the Rates of Ligand Binding Domain Closing and Opening Directly Impact AMPA Receptor Gating. *J. Neurosci. 28*, 932–943.
14. Burnashev, N., Monyer, H., Seeburg, P. H., and Sakmann, B. (1992) Divalent ion permeability of AMPA receptor channels is dominated by the edited form of a single subunit. *Neuron 8*, 189–198.
15. Greger, I. H., Khatri, L., Kong, X., and Ziff, E. B. (2003) AMPA receptor tetramerization is mediated by Q/R editing. *Neuron 40*, 763–774.
16. Swanson, G. T., Kamboj, S. K., and Cull-Candy, S. G. (1997) Single-channel properties of recombinant AMPA receptors depend on RNA editing, splice variation, and subunit composition. *J. Neurosci. 17*, 58–69.
17. Nanao, M. H., Green, T., Stern-Bach, Y., Heinemann, S. F., and Choe, S. (2005) Structure of the kainate receptor subunit GluR6 agonist-binding domain complexed with domoic acid. *Proc. Natl. Acad. Sci. U.S.A. 102*, 1708–1713.
18. Mayer, M. L. (2005) Crystal structures of the GluR5 and GluR6 ligand binding cores: Molecular mechanisms underlying kainate receptor selectivity. *Neuron 45*, 539–552.
19. Zhu, J. J., Esteban, J. A., Hayashi, Y., and Malinow, R. (2000) Postnatal synaptic potentiation: Delivery of GluR4-containing AMPA receptors by spontaneous activity. *Nat. Neurosci. 3*, 1098–1106.
20. Tai, L. S., Ng, T. K. Y., Mak, N. K., and Yung, K. K. L. (2001) Co-localization of AMPA-type glutamate receptor immunoreactivity in neurons of the rat subthalamic nucleus. *Brain Res. 895*, 95–103.
21. Hunter, C., Petralia, R. S., Vu, T., and Wenthold, R. J. (1993) Expression of AMPA-selective glutamate receptor subunits in morphologically defined neurons of the mammalian cochlear nucleus. *J. Neurosci. 13*, 1932–1946.
22. Wyllie, D. J., Traynelis, S. F., and Cull-Candy, S. G. (1993) Evidence for more than one type of non-NMDA receptor in outside-out patches from cerebellar granule cells of the rat. *J. Physiol. 463*, 193–226.
23. Monyer, H., Seeburg, P. H., and Wisden, W. (1991) Glutamate-operated channels: Developmentally early and mature forms arise by alternative splicing. *Neuron 6*, 799–810.
24. Mosbacher, J., Schoepfer, R., Monyer, H., Burnashev, N., Seeburg, P. H., and Ruppersberg, J. P. (1994) A molecular determinant for submillisecond desensitization in glutamate receptors. *Science 266*, 1059–1062.
25. Ying, H. S., Weishaupt, J. H., Grabb, M., Canzoniero, L. M. T., Sensi, S. L., Sheline, C. T., Monyer, H., and Choi, D. W. (1997) Sublethal Oxygen-Glucose Deprivation Alters Hippocampal Neuronal AMPA Receptor Expression and Vulnerability to Kainate-Induced Death. *J. Neurosci. 17*, 9536–9544.
26. Sommer, B., Keinänen, K., Verdoorn, T. A., Wisden, W., Burnashev, N., Herb, A., Köhler, M., Takagi, T., Sakmann, B., and Seeburg, P. H. (1990) Flip and flop: A cell-specific functional switch in glutamate-operated channels of the CNS. *Science 249*, 1580–1585.
27. Gill, A., and Madden, D. R. (2008) Purification and crystallization of a non-GluR2 AMPA-receptor ligand-binding domain: A case of cryo-incompatibility addressed by room-temperature data collection. *Acta Crystallogr. F64*, 831–835.
28. Kabsch, W. (1993) Automatic processing of rotation diffraction data from crystals of initially unknown symmetry and cell constants. *J. Appl. Crystallogr. 26*, 795–800.
29. Brünger, A. T., Adams, P. D., Clore, G. M., Delano, W. L., Gros, P., Grosse-Kunstleve, R. W., Jiang, J.-S., Kuszewski, J., Nilges, N., Pannu, N. S., Read, R. J., Rice, L. M., Simonson, T., and Warren, G. L. (1998) Crystallography and NMR system (CNS): A new software system for macromolecular structure determination. *Acta Crystallogr. D54*, 905–921.
30. Armstrong, N. A., and Gouaux, E. (2000) Mechanisms for activation and antagonism of an AMPA-sensitive glutamate receptor: Crystal structures of the GluR2 ligand binding core. *Neuron 28*, 165–181.
31. Cowtan, K. (1994) ′dm′: An automated procedure for phase improvement by density modification. *Joint CCP4 and ESF-EACBM Newsletter on Protein Crystallography 31*, 34–38.
32. Emsley, P., and Cowtan, K. (2004) Coot: Model-building tools for molecular graphics. *Acta Crystallogr. D60*, 2126–2132.
33. Collaborative Computational Project Number 4 (1994) The CCP4 suite: Programs for protein crystallography. *Acta Crystallogr. D50*, 760–763.
34. Winn, M. D., Isupov, M. N., and Murshudov, G. N. (2001) Use of TLS parameters to model anisotropic displacements in macromolecular refinement. *Acta Crystallogr. D57*, 122–133.
35. Kabsch, W. (1976) A solution for the best rotation to relate two sets of vectors. *Acta Crystallogr. A32*, 922–923.
36. Pettersen, E. F., Goddard, T. D., Huang, C. C., Couch, G. S., Greenblatt, D. M., Meng, C., and Ferrin, T. E. (2004) UCSF Chimera: A Visualization System for Exploratory Research and Analysis. *J. Comput. Chem. 25*, 1605–1612.
37. Yang, P., Jones, B. L., and Henderson, L. P. (2005) Role of the α subunit in the modulation of GABA(A) receptors by anabolic androgenic steroids. *Neuropharmacology 49*, 300–316.
38. Sun, Y., Olson, R., Horning, M., Armstrong, N., Mayer, M., and Gouaux, E. (2002) Mechanism of glutamate receptor desensitization. *Nature 417*, 245–253.
39. Lomeli, H., Mosbacher, J., Melcher, T., Hoger, T., Geiger, J. R., Kuner, T., Monyer, H., Higuchi, M., Bach, A., and Seeburg, P. H. (1994) Control of kinetic properties of AMPA receptor channels by nuclear RNA editing. *Science 266*, 1709–1713.
40. Krampfl, K., Schlesinger, F., Zorner, A., Kappler, M., Dengler, R., and Bufler, J. (2002) Control of kinetic properties of GluR2 flop AMPA-type channels: Impact of R/G nuclear editing. *Eur. J. Neurosci. 15*, 51–62.
41. Greger, I. H., Akamine, P., Khatri, L., and Ziff, E. B. (2006) Developmentally regulated, combinatorial RNA processing modulates AMPA receptor biogenesis. *Neuron 51*, 85–97.
42. Stern-Bach, Y., Russo, S., Neuman, M., and Rosenmund, C. (1998) A point mutation in the glutamate binding site blocks desensitization of AMPA receptors. *Neuron 21*, 907–918.

43. Greger, I. H., Ziff, E. B., and Penn, A. C. (2007) Molecular determinants of AMPA receptor subunit assembly. *Trends Neurosci. 30*, 407–416.
44. Jayaraman, V., Keesey, R., and Madden, D. R. (2000) Ligand-protein interactions in the glutamate receptor. *Biochemistry 39*, 8693–8697.
45. Madden, D. R., Cheng, Q., Thiran, S., Rajan, S., Rigo, F., Keinänen, K., Reinelt, S., Zimmermann, H., and Jayaraman, V. (2004) The stereochemistry of glutamate receptor agonist efficacy: Engineering a dual-specificity AMPA/kainate receptor. *Biochemistry 43*, 15838–15844.
46. Madden, D. R., Thiran, S., Zimmermann, H., Romm, J., and Jayaraman, V. (2001) Stereochemistry of quinoxaline antagonist binding to a glutamate receptor investigated by Fourier transform infrared spectroscopy. *J. Biol. Chem. 276*, 37821–37826.
47. Abele, R., Keinänen, K., and Madden, D. R. (2000) Agonist-induced isomerization in a glutamate receptor ligand-binding domain: A kinetic and mutagenetic analysis. *J. Biol. Chem. 275*, 21355–21363.
48. Keinänen, K., Wisden, W., Sommer, B., Werner, P., Herb, A., Verdoorn, T. A., Sakmann, B., and Seeburg, P. H. (1990) A family of AMPA-selective glutamate receptors. *Science 249*, 556–560.
49. Armstrong, N., Mayer, M., and Gouaux, E. (2003) Tuning activation of the AMPA-sensitive GluR2 ion channel by genetic adjustment of agonist-induced conformational changes. *Proc. Natl. Acad. Sci. U.S.A. 100*, 5736–5741.
50. Jin, R., and Gouaux, E. (2003) Probing the function, confomational plasticity, and dimer-dimer contacts of the GluR2 ligand-binding core: Studies of 5-substituted willardiines and GluR2 S1S2 in the crystal. *Biochemistry 42*, 5201–5213.
51. Frandsen, A., Pickering, D. S., Vestergaard, B., Kasper, C., Nielsen, B. B., Greenwood, J. R., Campiani, G., Fattorusso, C., Gajhede, M., Schousboe, A., and Kastrup, J. S. (2005) Tyr702 Is an Important Determinant of Agonist Binding and Domain Closure of the Ligand-Binding Core of GluR2. *Mol. Pharmacol. 67*, 703–713.
52. Jane, D. E., Hoo, K., Kamboj, R., Deverill, M., Bleakman, D., and Mandelzys, A. (1997) Synthesis of Willardiine and 6-Azawillardiine Analogs: Pharmacological Characterization on Cloned Homomeric Human AMPA and Kainate Receptor Subtypes. *J. Med. Chem. 40*, 3645–3650.
53. Stensbøl, T. B., Madsen, U., and Krogsgaard-Larsen, P. (2002) The AMPA Receptor Binding Site: Focus on Agonists and Competitive Antagonists. *Curr. Pharm. Des. 8*, 857–872.
54. Jensen, A. A., Christesen, T., Bolcho, U., Greenwood, J. R., Postorino, G., Vogensen, S. B., Johansen, T. N., Egebjerg, J., Brauner-Osborne, H., and Clausen, R. P. (2007) Functional Characterization of Tet-AMPA [Tetrazolyl-2-amino-3-(3-hydroxy-5-methyl- 4-isoxazolyl)propionic Acid] Analogues at Ionotropic Glutamate Receptors GluR1-GluR4. The Molecular Basis for the Functional Selectivity Profile of 2-Bn-Tet-AMPA. *J. Med. Chem. 50*, 4177–4185.
55. Potterton, L., McNicholas, S., Krissinel, E., Gruber, J., Cowtan, K., Emsley, P., Murshudov, G. N., Cohen, S., Perrakis, A., and Noble, M. (2004) Developments in the CCP4 molecular-graphics project. *Acta Crystallogr. D60*, 2288–2294.

BI8013196